PROSIDING SNTTM XXIII 2025
Volume 23, No. 1, Tahun 2025, 9 Oktober 2025
e-ISSN 2623-0313
p-ISSN 3032-1972

Impact of flow regimes and coarse fly ash particle dynamics in circular slurry transport using CFD–DEM

Yanuar[a], Raja Fatah Satrio Abimanyu[a, 1], Chakra Merdeka[a], Gunawan[a], Sri Poernomo Sari[b]

[a]Department of Mechanical Engineering, Universitas Indonesia, Depok, 16424, Indonesia
[b]Department of Mechanical Engineering, Gunadarma University, Depok, 16424, Indonesia
[1]E-mail correspondent: raja.fatah51@ui.ac.id

Abstract. Fly ash is one of the major solid residues produced from coal combustion in power plants and presents significant environmental challenges due to its large volume and complex handling requirements. One promising mitigation approach is transporting fly ash as a slurry through pipeline systems. However, efficient slurry transportation remains challenging due to the high concentration of suspended particles, which significantly influences flow behavior and energy consumption. This study investigates the flow characteristics and energy demand of fly ash slurry transported through circular pipelines using a combined experimental and Computational Fluid Dynamics–Discrete Element Method (CFD–DEM) approach. Slurry concentrations of 30%, 40%, and 50% by weight were analyzed under turbulent flow conditions with a Reynolds number of approximately 50,000. Key flow parameters examined include pressure drop, velocity distribution, and turbulent kinetic energy (TKE) to better understand particle–fluid interactions within the pipeline. The results show that increasing solid concentration significantly affects the hydrodynamic characteristics of the slurry flow. At 30% concentration, the pressure drop is relatively low (approximately 652 Pa), but the turbulence intensity is insufficient to maintain full particle suspension. At 40% concentration, the pressure drop increases to approximately 2660 Pa, creating a more stable flow condition in which particles remain suspended while maintaining moderate energy consumption. At 50% concentration, the pressure drop reaches approximately 3251 Pa, accompanied by a peak turbulent kinetic energy of 0.086, indicating strong particle interactions and increased energy demand. The CFD results show good agreement with experimental measurements, with deviations of 6.21%, 4.16%, and 5.03% for the respective concentrations. A Grid Convergence Index (GCI) of 0.017% further confirms the numerical reliability. These findings provide important insights for improving the efficiency and reliability of fly ash slurry transport systems.

Keywords: *fly ash, CFD-DEM, rheology, GCI, erosion.*

Received: 30 September 2025; **Presented:** 9 October 2025; **Publication:** 9 March 2026
DOI: https://doi.org/10.71452/yd51zd47

INTRODUCTION

Coal remains one of the most important energy sources in modern power generation in Indonesia [1], coal plays a dominant role in meeting national electricity demand, particularly through coal-fired power plants (PLTU) [2]. The operating principle of coal-based systems involves burning solid fuels such as coal or gas to generate thermal energy, which is then used to heat water in a boiler to produce steam [3].

One of the combustion technologies widely applied in PLTU is the fluidized bed system. In this method, air is blown from below using a blower, causing solid particles to behave like a fluidized medium. While this system is considered efficient for energy production, it also generates large quantities of solid waste, most notably fly ash [4]. As the number of coal-fired power plants in Indonesia continues to grow, the production of fly ash has increased significantly, from 1.66 million tons in 2000 to nearly 2 million tons in 2006, and is expected to rise further in line with coal consumption across various industrial sectors [5].

One proposed strategy for handling fly ash is to transport it as a slurry, a mixture of fly ash and water, through long-distance pipeline systems. However, this method faces fundamental challenges, such as particle sedimentation, flow blockage, reduced transport efficiency, and increased energy consumption [6]. These challenges become more critical when dealing with high solid concentrations, highlighting the need for more efficient hydraulic designs [7]. Conventional circular pipes typically require high flow velocities to prevent sedimentation; however, this approach is energy-inefficient because it results in significant pressure losses and increased pumping power requirements [8]. Recent studies have shown that applying multi-stage reducers and optimizing pipe geometries can effectively reduce pressure drop and improve slurry transport efficiency [9]. Therefore, the exploration of alternative pipe designs that can more effectively mitigate sedimentation is urgently required.

A comprehensive understanding of flow regime characteristics and particle dynamics is essential in designing efficient slurry transport systems [10]. Flow regimes inside pipelines ranging from fixed bed flow to sliding flow strongly influence transport efficiency and sedimentation behavior [11]. These regimes depend on several parameters, including flow velocity, slurry viscosity, particle physical properties, and pipe

e-ISSN 2623-0313
p-ISSN 3032-1972

geometry. To address this complexity, advanced numerical modeling and pilot-scale loop experiments have been widely applied, allowing more accurate predictions of flow behavior and system performance [12]. Insufficient understanding of these dynamics can lead to suboptimal system designs, higher risks of blockage, and greater energy consumption.

In this study, experiments were conducted to observe the behavior of fly ash slurry flow in pipelines with different geometries, namely circular pipes [13]. The main objectives were to characterize particle–fluid interactions, evaluate sedimentation risks, and assess transport efficiency under various operating conditions. The experimental setup was designed with sufficient pipe length to ensure steady-state flow before measurement. A pitot tube was used to obtain velocity distribution, while pressure sensors were employed to record pressure profiles and energy losses due to wall friction [14].

The slurry consisted of fly ash mixed with water, with solid concentrations of 30%, 40%, and 50% by weight. Chemical composition analysis showed that fly ash contains 54.32% SiO_2, 31.58% Al_2O_3, 3.66% Fe_2O_3, along with smaller fractions of MgO, SO_3, K_2O, P_2O_5, and TiO_2. The high silica (SiO_2) content suggests an abrasive tendency, while the relatively high Fe_2O_3 and SO_3 contents indicate strong chemical reactivity. Meanwhile, the presence of Al_2O_3 imparts thermal resistance and durability to fly ash in alkaline environments. These compositional characteristics directly influence slurry viscosity, stability, and transport behavior in pipelines [9].

In addition to experimental approaches, numerical modeling using Computational Fluid Dynamics (CFD) and the Discrete Element Method (DEM) has become an important tool for studying solid–liquid two-phase flows [12]. CFD with a mixture flow regime and turbulence modeling, such as k–ω SST, enables accurate analysis of slurry flows, particularly in predicting pressure distribution and particle concentration [15], although it has limitations in describing direct particle interactions [10]. DEM complements this by enabling detailed analysis of individual particle trajectories and interactions with fluid and pipe walls [16]. The combined CFD–DEM framework provides a comprehensive analytical approach: CFD delivers macroscopic insight into the flow field, while DEM captures microscopic particle dynamics such as trajectories and transient forces, which are difficult or even impossible to measure experimentally [17, 18]. This integrated approach allows a more complete understanding of fly ash slurry flow regimes and supports the development of more efficient transport systems.

METHODS

Experimental Setup

The experimental setup used in this study is illustrated in Figure 1. The system configuration follows the baseline design previously investigated by Yanuar [8], in which the hydraulic performance of a slurry transport pipeline was evaluated using a circular pipe geometry. The experimental apparatus consists of a main mixing tank, a centrifugal pump, a circular test pipe, and a discharge tank. The circular test pipe has a total length of 1100 mm, with an inner diameter of 36 mm and an outer diameter of 42 mm. The slurry mixture is prepared in the mixing tank and circulated through the pipeline system using the centrifugal pump to ensure continuous flow during the experiment. To evaluate hydraulic performance, two pressure transducers are installed at the upstream and downstream ends of the test pipe to measure the pressure drop due to slurry viscosity and internal friction along the pipe wall. The distance from the pipe inlet to the first measurement location is 130 mm. This inlet length is designed to allow the flow to develop fully before entering the test section, thereby ensuring accurate pressure measurements under fully developed flow conditions.

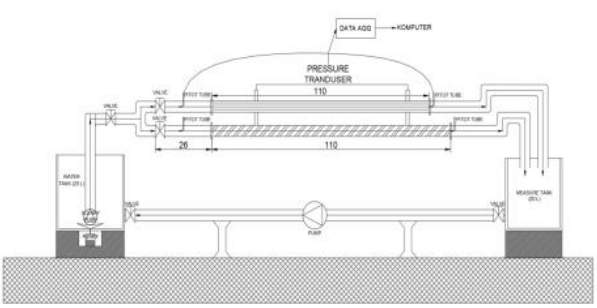

Figure 1. Experimental Setup

The total internal volume of the circular test pipe is 4.476 L. Prior to operation, the sealed pipeline system is filled with water to prevent leakage and to establish stable initial operating conditions. During the experiment, the slurry flows continuously from the mixing tank through the test pipe and is subsequently collected in the discharge tank. This circular pipe configuration serves as the reference case for evaluating the baseline hydraulic characteristics of slurry transport. The experimental results obtained from this setup are later used as a benchmark for comparison with alternative pipe geometries.

Pipe Configuration and Slurry Properties for Experiment and Simulation

In the experimental study, the pump was operated at a constant power of 25 W, while the flow rate was controlled by maintaining a fixed valve opening. The pump used in this study was a Sewage Submersible

e-ISSN 2623-0313
p-ISSN 3032-1972

Pump V250, which has a maximum capacity of 9 m³/h and a maximum head of 7.5 m. Two types of working fluids were used, namely water and fly ash slurry. The slurry was prepared with three different solid concentrations (Cw), namely 30%, 40%, and 50% by weight. These variations were selected to evaluate the influence of solid concentration on flow characteristics under turbulent conditions. The experimental data were analyzed using rheological methods to characterize the slurry's non-Newtonian behavior. The operating conditions and key parameters used in the experiment are summarized in **Table 1.**

Table 1. Case Parameter Setting of Experiment (Re = 50000).

Circular Fly Ash			
Volume Fraction (%)	30%	40%	50%
Velocity Inlet (m/s)	1.301139	2.9115772300	3.063218808
Velocity Outlet (m/s)	1.638227	3.5477037400	3.700317860
Pressure Drop (pa)	782.457412	2537.946	4544.8906
Reynolds Number	50823.7509	50765.0368	50836.3
Flow Rate (Kg/s)	0.00167	0.003597	0.0045475
Mass Flow Rate (Kg/s)	4.0922	5.011	8.23

Mathematical Model

The CFD–DEM approach is applied to analyze particle transport behavior in fly ash slurry flow within a circular pipe. In this method, the slurry consisting of water and fine particles is treated as a continuous phase using the CFD mixture model, while coarse particles are modeled as a discrete phase using the Discrete Element Method (DEM). This approach enables simultaneous analysis of macroscopic flow characteristics and microscopic particle dynamics. The simulation captures key particle transport mechanisms, including suspension, settling, and rolling, which are influenced by variations in velocity, particle concentration, and particle size, thereby determining the velocity distribution and particle dispersion across the pipe cross-section.

The DEM model is based on Newton's laws of motion to calculate particle trajectories, considering forces such as drag, gravity, and collision interactions between particles and pipe walls. The CFD model employs the k–ω SST turbulence model to accurately capture turbulent flow behavior, particularly near the wall region. The coupling between CFD and DEM allows the exchange of momentum, mass, and energy between phases, where the fluid field influences particle motion and particle interactions provide feedback to the fluid domain. This coupled framework provides a reliable approach for predicting slurry flow behavior and optimizing pipeline transport performance.

CFD Fluid and Particle Phase Modeling

The mixture model for transient Navier–Stokes equations is widely used to simulate multiphase flows in which the phases share a common velocity field with low slip velocities. This model provides a balance between computational efficiency and accuracy in capturing multiphase interactions [19]. The governing equations are based on the Navier–Stokes equations, which are fundamental for solving flow problems in CFD simulations [21]. The continuity equation for the mixture is expressed as

$$\frac{\partial \rho_m}{\partial t} + \nabla.(\rho_m U_m) = 0 \quad (1)$$

where, $\rho_{m=\sum_i \propto_i \rho_i}$ represents the mixture density, $\propto_i$ is the volume fraction of phase i, and U_m is the mixture velocity. The momentum equation is given by:

$$\frac{\partial}{\partial t}(\rho_m U_m) + \nabla.(\rho_m U_m U_m) = -\nabla P + \nabla.(\mu_m \nabla U_m) + \rho_m g + \sum_i \propto_i \rho_i F_i \quad (2)$$

e-ISSN 2623-0313
p-ISSN 3032-1972

where P is pressure, $\mu_m = \sum_i \propto_i \mu_i$ is the mixture viscosity, g is gravitational acceleration, and F_i accounts for interphase forces such as drag. Various multiphase Navier-Stokes formulations have been proposed to describe non-matching density mixtures, yet a unified modelling approach remains absent [20]. The volume fraction equation for each phase follows

$$\frac{\partial \propto_i}{\partial t} + \nabla.(\propto_i U_m) + \nabla.(\propto_i U_{slip,i}) = 0, \quad (3)$$

where $U_{slip,i} = U_i - U_m$ represents the slip velocity between the phase and the mixture. Additionally, in the momentum equation of the Mixture Model, this study employs the turbulent kinetic energy (k) and specific dissipation rate (ω) transport equations as defined in the k-ω SST (Shear Stress transport) model. The turbulent viscosity is defined as $\mu_{t=} \frac{\rho k}{\omega}$ and the Boussinesq hypothesis is applied to model the turbulent viscous forces. This substitution allows the viscous terms in the momentum equations to be rewritten, resulting in the transport equations for the mixture model being expressed in terms of k-ω SST while incorporating the volume fraction $\propto_i$ of each phase:

$$\rho_m k_m = \sum_i \propto_i \rho_i k_i \text{ and } \rho_m \omega_m = \sum_i \propto_i \rho_i \omega_i \quad (4)$$

The mixture model using k - ω SST is typically employed in ANSYS Fluent for multiphase flows with low interphase slip, such as slurry transport, sediment transport, and bubbly flows with low gas fractions. This approach offers a balance between computational efficiency and accuracy, making it suitable for engineering applications where tracking individual phases explicitly is unnecessary.

DEM Particle Phase Modeling

The Discrete Element Method (DEM) is employed to simulate the motion and interactions of discrete particles within a fluid environment. DEM tracks individual particle trajectories based on Newton's second law, formulated as: The governing equations for the translational and rotational motions of the particles within the pipe are as follows [10]:

$$m_\rho = \frac{dv_p}{dt} = \sum F \quad (5)$$

where m_ρ is the particle mass, v_p is the velocity, and $\sum F$ represents the total forces acting on the particle. These forces include the drag force F_{drag} , lift force F_{lift} gravitational force $F_{gravity}$, and collision forces $F_{colison}$ based on the Hertz-Mindlin contact model. The rotational motion of particles is determined using:

$$I_\rho \frac{d\omega_\rho}{dt} = m_\rho \quad (6)$$

where I_ρ is the moment of inertia, ω_ρ is the angular velocity, and m_ρ is the torque due to contact forces.

Interfacial Forces

The interaction between the fluid phase (CFD) and the particle phase (DEM) is governed by interfacial forces, representing the velocity difference between the phases and the mixture [21]. including :

$$F_B = (\rho_f - \rho_P) g V_P \quad (7)$$

e-ISSN 2623-0313
p-ISSN 3032-1972

where F_B is the buoyancy force ρ_f and ρ_P are the densities of fluid and particles, respectively, and V_P is the particle volume.

$$F_D = \frac{18\mu_e}{\rho_P d_P^2} C_D Re_P (U_f - U_P) \quad (8)$$

where C_D is the drag coefficient, Re_P is the particle Reynolds number, and μ_e is the effective viscosity.

$$F_P = -\frac{1}{\rho_P} \nabla P \quad (9)$$

$$U_{slip,i} = U_i - U_m \quad (10)$$

where, F_P is Pressure Gradient Force and $U_{slip,i}$ is slip velocity

Wall Function

The wall function approach is used to model near-wall turbulence effects and particle wall interactions in CFD-DEM simulations. This is particularly important in the k-ω SST turbulence model, where turbulence viscosity near the wall is modeled using logarithmic wall functions [21]:

$$U^+ = \frac{1}{k} ln(y^+) + C \quad (11)$$

where U^+ is the non-dimensional velocity, k is the von Kármán constant, and y^+ is the non-dimensional wall distance. For particle-wall interactions, the Hertz-Mindlin contact model is used:

$$F_n = k_n \delta_n + C_n v_n \quad (12)$$

$$F_t = min(\mu_s F_n k_t \delta_t + C_t v_t) \quad (13)$$

where k_n and k_t are normal and tangential stiffness, δ_n and δ_t are normal and tangential overlaps, and C_n and C_t are damping coefficients.

Coupling Process

The CFD-DEM coupling integrates Mixture-based fluid modeling (CFD) with Lagrangian-based particle modeling (DEM). To capture the detailed process of the interaction between the liquid and solid phases, the coupling process is implemented by initializing the boundary conditions for the fluid domain in ANSYS Fluent and the solid-phase particles defined in the Rocky DEM environment. Once the system is initialized, the simulation is run in a sequence of time steps. Since the solid-phase interaction requires higher time resolution, for each CFD time step, multiple DEM sub-time steps are performed to capture particle dynamics.

Then, a force-exchange mechanism occurs, in which the CFD solver calculates the flow field and interpolates the velocity, pressure, and turbulence properties onto each DEM particle. The DEM solver then uses these interpolated values to calculate the interaction forces acting on the particles, updating their motion and position accordingly. This computational loop of fluid calculation, force interpolation, and particle update is then repeated until both the fluid and particle domains reach the steady states.

This coupling approach enables an accurate representation of multiphase flow interactions, especially in complex applications such as slurry transport, sediment transport, and turbulent particle-laden flows. The use of the k-ω SST turbulence model in ANSYS Fluent further enhances near-wall flow

e-ISSN 2623-0313
p-ISSN 3032-1972

resolution, contributing to more reliable simulations of fluid-particle dynamics.

Table 2. Parameter Setting of Control Group in CFD – DEM Coupling Simulation on Fly Ash

Parameter	Input Value
	Fly Ash
Particles Density (kg/m^3)/Bulk Density	1780
Particle Diameter(m)	1x10^{-3}
Specific Dissipation Rate[s^{-1}]	Cw 30% = 683.4509 Cw 40% =1241.672 Cw 50% =1115.457
Turbulent Kinetic Energy[m^2/s^2]	Cw 30% = 0.01029739 Cw 40% =0.03389762 Cw 50% = 0.04246381

Grid Independence Convergence Verification

The GCI (Grid Convergence Index) results approaching 1 indicate a stable, convergent, and valid solution with a very high level of accuracy. The Grid Convergence Independence analysis results show that the optimal mesh element count for the circular pipe is 1,032,324, with a cell size of 0.001456411 meters and an error rate of 0.017432%. The skewness value of 0.9 indicates a slight asymmetry in the data distribution for circular pipes.

Boundary Condition

In this simulation, the Mixture model is used as the multiphase model to represent the flow as a slurry, with solid and liquid phases fully accounted for by a single mixture momentum equation to maintain computational efficiency and stability. The CFD model accounts for different turbulence, granular-flow, and numerical-discretization models to predict realistic flows. The volume fraction parameters are modeled using the Implicit Scheme, and viscous modeling is carried out using the k−ω SST turbulence model to better capture near-wall interaction effects. The granular phase interactions are described based on the Syamlal-O'Brien model for viscosity and radial distribution, the Lun et al. bulk viscosity and solid pressure model, and the Johnson et al.

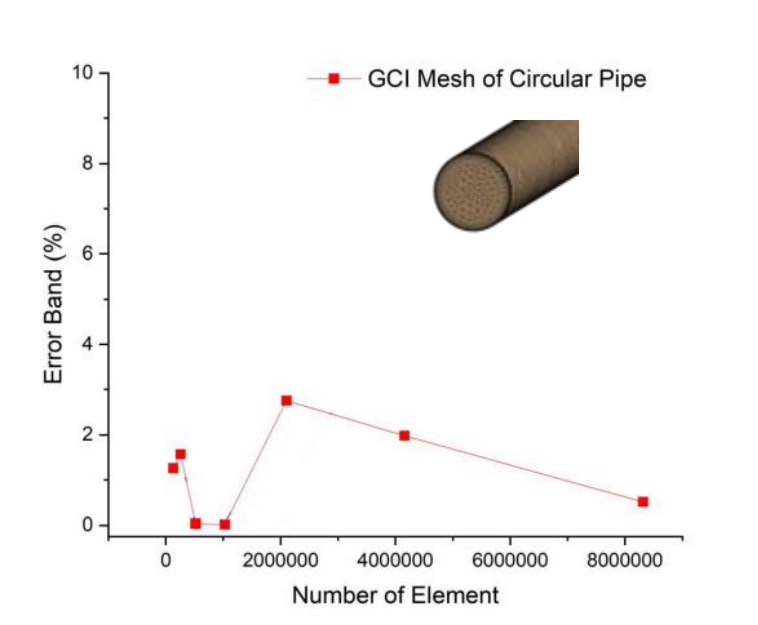

Figure 2. GCI Verification

e-ISSN 2623-0313
p-ISSN 3032-1972

Table 3. Parameter Setting of Control Group in CFD – DEM Coupling Simulation

Check Mesh Quality	Yes, Errors
Target Skewness	Default (0.9)
Smoothing	Medium
Mesh Metric	Orthogonal Quality
Min	0.22932
Max	0.99171
Average	0.80627
Standard Deviation	9.1248e-002

Model force interaction is applied for phase interaction, utilizing the frictional pressure-based model, Based-KTGF, and the Algebraic model for granular temperature. SIMPLE Scheme for pressure velocity coupling, Least Squares Cell-Based discretization for gradients, and PRESTO! for pressure, Second Order Upwind for momentum, turbulent kinetic energy and specific dissipation rate, and Compressive for volume fraction. collisions within the phase are also accounted for, the Schiller-Naumann drag coefficient with Wall-Drag Enhancement, the Manninen et al. slip-velocity model, and a constant surface-tension coefficient of 0.072 N/m in the Continuum Surface Force method with Wall Adhesion. Pseudo Time is also off, and the First Order Implicit transient formulation is employed to balance computational cost and solution accuracy in CFD simulations.

Rheological Modeling

The rheological properties of the slurry were analyzed. The fluid characteristic obtained from experimental data is plotted in the Moody chart. Laminar region refers to the Hagen-Poiseuille line, and the turbulent region refers to the Prandtl-Karman line [8]. Power law model used in non-Newtonian fluid model, with the relation between shear stress (τ) and shear rate (γ) is proportional as follows:

$$\tau = K(\gamma)^n \tag{14}$$

These parameters were subsequently input into the CFD software for simulation calculations.

Table 4. Fly Ash Power Law Model

Fluid	***K***	***n***
Fly Ash Cw=30%	0.001555	0.90
Fly Ash Cw=40%	0.002892	*0.93*
Fly Ash Cw=50%	0.0038	*0.96*

Experiment Validation of The Model

Figure 3 highlights the performance of the CFD–DEM–DPM multiphase simulation in replicating the flow behavior of fly ash slurry under turbulent conditions in a circular pipe. The simulation model shows strong agreement with experimental data, with all deviations remaining well below 10%. Specifically, the deviations are 6.21% (FA 30%), 4.16% (FA 40%), and 5.03% (FA 50%).

These values demonstrate the reliability and robustness of the coupled CFD–DEM–DPM approach in modeling dense slurry flows, particularly in capturing particle–fluid interactions, wall-bounded behavior, and turbulence-induced dispersion. The consistent validation across varying solid concentrations confirms the model's ability to represent complex rheological responses and heterogeneous particle–fluid interactions.

This performance is in line with, and even expands upon, previous work by Singh et al. [7], who reported a minimum deviation of 6.81% using SST k-ω modeling for coal–water slurry systems. While Singh's study was limited to a single turbulence model, the present work demonstrates comparable or better

e-ISSN 2623-0313
p-ISSN 3032-1972

accuracy across multiple concentration levels, reinforcing the applicability of CFD–DEM–DPM in real-world process engineering contexts.

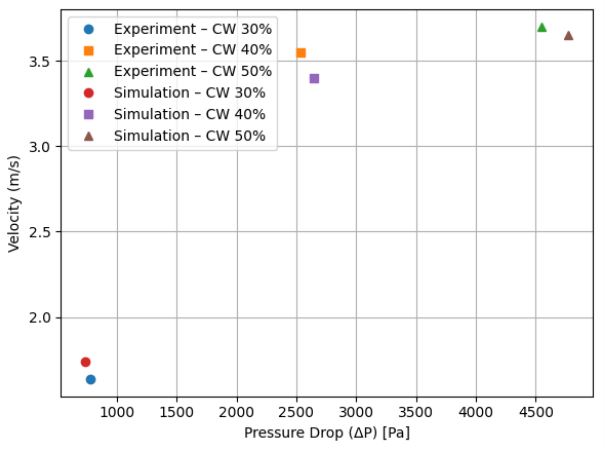

Figure 3. Experiment Validation

RESULTS AND DISCUSSION

Analysis of Pressure Fly Ash Distribution of Slurry at Circular Pipe and Different Volume Fractions

The pressure distribution of fly ash slurry in circular pipes is strongly governed by solid concentration, flow regime, and particle–fluid interactions. At low concentration (30% CW), the pressure drop is minimal (651.6 Pa), reflecting low hydrodynamic resistance and reduced pumping energy requirements. However, the limited turbulence at this level provides insufficient suspension force, allowing particles to settle at the pipe bottom. This condition represents a transitional regime between laminar and turbulent flow, where stratification and instability are more likely to occur.

At medium concentration (40% CW), the pressure drop increases to 2,660 Pa, indicating stronger turbulence that effectively suspends particles throughout the pipe cross-section. The flow exhibits a more balanced hydraulic condition, maintaining particle suspension without incurring excessive energy losses. This scenario represents the most stable and efficient transport condition for fly ash slurry.

At high concentration (50% CW), the largest pressure drop is observed (3,250.8 Pa), caused by increased slurry density, frequent particle–particle collisions, and intensified particle-wall interactions. The flow exhibits a shear-thinning response, with viscosity decreasing as shear rate increases, accompanied by high turbulence and localized vortices near the wall. While this condition ensures effective suspension, it demands higher pumping power and significantly increases the risk of pipe wall erosion.

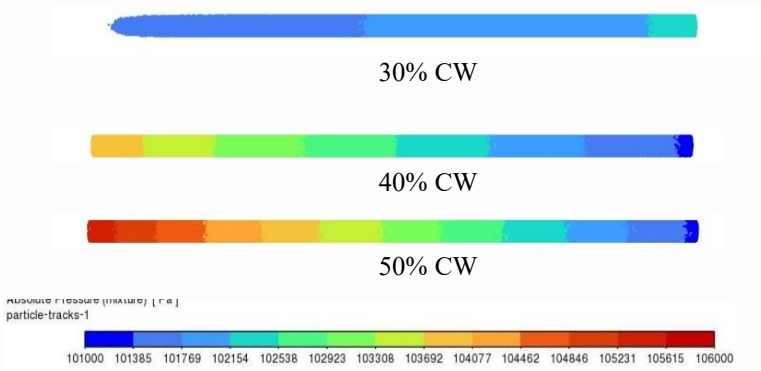

Figure 4. Fly Ash Pressure in Circular Pipe

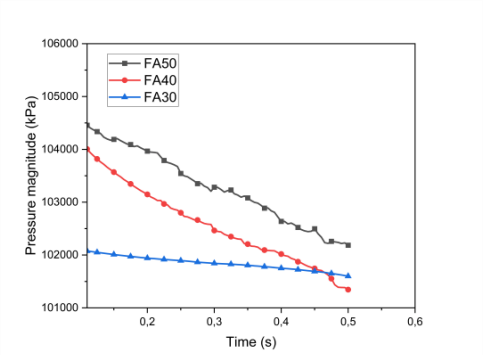

Figure 5. Graph of Fly Ash Pressure

e-ISSN 2623-0313
p-ISSN 3032-1972

Analysis of Velocity Fly Ash Distribution of Slurry at Circular Pipe and Different Volume Fractions

The velocity contour visualization in **Figure 6** illustrates the dynamic evolution of slurry flow characteristics as the fly ash concentration increases across three volume fractions (Cw = 30%, 40%, and 50%) under fully turbulent conditions (Re = 50,000). The contour gradients, ranging from blue (low velocity) to red (high velocity), depict variations in flow intensity throughout the pipe cross-section. The flow analysis conducted at x = 0.9 meters, located near the pipe outlet, offers a representative depiction of the slurry's final hydrodynamic behavior after traversing the entire pipe length within the 0.5-second simulation timeframe under steady-state conditions

At 30% Cw for fly ash, the velocity remains under 2.5 m/s, dominated by light cyan hues, and displays a symmetric distribution of particles suspended closer to the pipe centerline, with consistent particle velocities and minimal deposition along the pipe's lower wall, typical of a sliding bed regime. Turbulent intensity and shear gradients are minimal at this stage, and there is no significant evidence of secondary flow or vortex formation within the slurry stream, indicating a relatively orderly flow structure.

As the concentration increases to 40% Cw, the core velocity rises to approximately 3.5 to 4.0 m/s. The flow shifts toward a transition regime; this shift is visualized by the transition from green to yellow shades near the pipe center. The flow begins transitioning toward a turbulent regime, with steeper velocity gradients forming near the wall. These changes suggest the onset of weak secondary flows or the early development of vortices, although the flow direction remains predominantly axial.

At the highest concentration of 50% Cw, the velocity distribution undergoes a marked transformation. The core velocity reaches 5.5–6.0 m/s, evidenced by bright yellow and pale orange regions at the center. Meanwhile, dark blue zones near the wall indicate flow velocities below 1.5 m/s, signifying a sharp radial gradient. This scenario corresponds to a shear-dominated or fixed/dense-bed regime, characterized by well-defined shear layers and significant velocity gradients between the core and boundary regions. These conditions promote the formation of rotational vortices at the core boundary interface, which are essential for maintaining particle suspension but may also lead to localized recirculation near the pipe wall. Although streamline plots are not explicitly shown, the velocity profile and contour geometry strongly suggest the presence of tangential flow components, a defining feature of secondary vortex structures in dense, non-Newtonian slurry flows under turbulent shear.

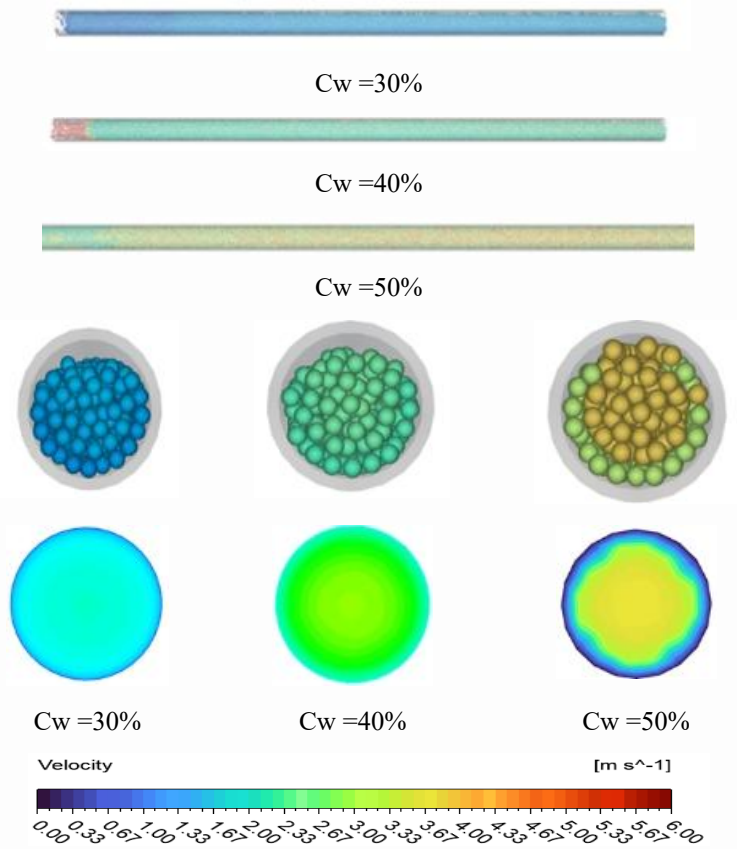

Figure 6. Fly Ash Velocity in Circular Pipe

e-ISSN 2623-0313
p-ISSN 3032-1972

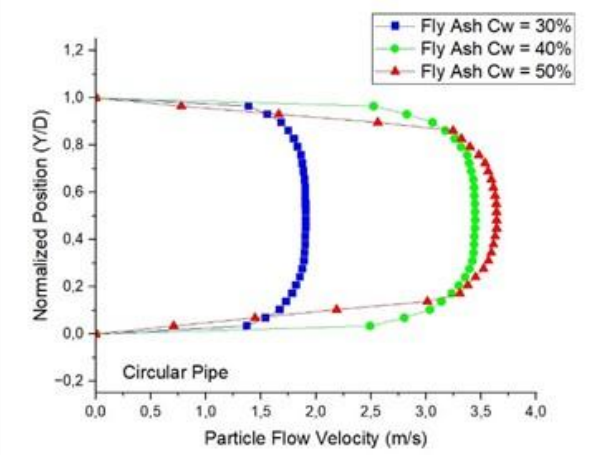

Figure 7. Particle Flow Velocity

Figure 7 presents the distribution of particle velocity in fly ash slurry flowing through a circular pipe under fully developed turbulent conditions, with a Reynolds number set at 50,000. Despite the fluid flow rate being held constant throughout the simulation, increasing the slurry concentration significantly elevates the dynamic viscosity, which in turn modifies the internal flow structure and the resulting velocity profiles.

At Cw = 30%, the dynamic viscosity is relatively low, resulting in a highly centralized flow regime. The velocity profile exhibits a symmetrical parabolic shape with a peak velocity of around 2.5 m/s, concentrated along the pipe's central axis.

As the solid content increases to Cw = 40%, the elevated viscosity thickens the near-wall boundary layer, leading to a wider radial spread of velocities. Under these conditions, the maximum velocity reaches approximately 3.3 m/s, indicating a partial redistribution of flow momentum away from the center.

At the highest tested concentration, Cw = 50%, the dynamic viscosity reaches its maximum, promoting the development of steep velocity gradients and intensified shear near the pipe walls. This encourages a shift in flow energy toward the outer radial regions, accelerating particles further from the core and pushing the peak velocity beyond 3.5 m/s. The resulting velocity field displays characteristics of a shear-driven flow regime with increased radial heterogeneity.

The imposed Reynolds number of 50,000 enhances the influence of these phenomena, as the flow resides within a turbulence-dominated regime where inertial effects are pronounced. The velocity distribution becomes increasingly blunted and radially diffused, effectively enlarging the cross-sectional area contributing to particle transport. This change may lead to a higher volumetric flow rate. Additionally, under high concentration conditions, the interaction between elevated viscosity and sharp velocity gradients can give rise to localized instabilities, fostering the development of secondary flows or vortices. These dynamic structures influence the spatial distribution of particles and may increase the likelihood of deposition zones or pipe wall erosion over time.

Analysis of Vortex Fly Ash Distribution of Slurry at Circular Pipe and Different Volume Fractions

Figure 8 illustrates contour distributions of turbulent intensity for fly ash slurry flows inside a circular pipe, analyzed across three solid volume concentrations (Cw = 30%, 40%, and 50%). The vortex evaluation performed at the x = 0.9 meter position, proximal to the pipe outlet, provides a representative depiction of the slurry's final hydrodynamic behavior after traversing the entire pipe length within the 0.5-second simulation timeframe under steady-state conditions. The color mapping reflects the magnitude of velocity fluctuations relative to the local mean velocity, with red areas indicating zones of maximum turbulence intensity (reaching approximately 7.25e+00), while blue areas represent regions with minimal fluctuation (approaching zero).

For fly ash, at a concentration of Cw = 30%, the flow is in an early transitional regime. Turbulent intensity is localized near the pipe wall with symmetrical contours, indicating the formation of Dean circulation type I, characterized by a pair of small, symmetric counter-rotating vortices along the wall. These vortices are limited in scale and maintain a balanced rotational structure.

As the concentration increases to Cw = 40%, the turbulent intensity distribution begins to exhibit asymmetric deformation in the contour plot. The thickening of red zones near the pipe wall, along with intrusions of velocity fluctuations toward the core

e-ISSN 2623-0313
p-ISSN 3032-1972

region, suggests the development of Deformed Dean circulation type II. This circulation is identified by two vortices rotating in opposite directions that are no longer symmetrical, reflecting the growing influence of shear forces as inertial effects begin to outweigh viscous damping.

At Cw = 50%, the turbulent contours display further deformation and strong spatial irregularities. Bright red intensity zones dominate not only the boundary layer but also begin to penetrate the pipe core, indicating the emergence of more complex vortex structures. This pattern corresponds to Intermediate circulation type III or potentially approaches Deformed Lyne circulation type IV, where vortices become non-symmetric and begin to shift, forming micro-spiral rotation patterns due to the imbalance between shear stress and local centrifugal forces. This phenomenon is indicative of a transition to a fully turbulent regime, in which the flow exhibits multidirectional instabilities.

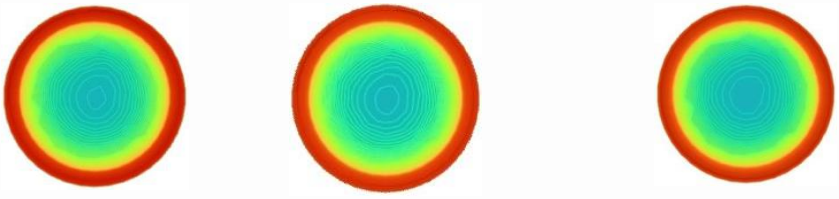

30% CW 40% CW 50% CW

Figure 8. Fly Ash Vortex in Circular Pipe

Analysis of Erosion Fly Ash Distribution of Slurry at Circular Pipe and Different Volume Fractions

The performance analysis of fly ash slurry flow in circular pipes at three concentration variations (Cw 30%, 40%, and 50%) reveals significant differences in particle accumulation, flow velocity, turbulence levels, and pipe wall erosion potential. Figure (a) presents the trend in the number of particles reaching the pipe outlet over time for slurry concentrations of Cw 30%, 40%, and 50%. The FA 50% curve demonstrates the most rapid accumulation, indicating that a higher solid volume fraction facilitates faster particle transport due to increased momentum and flow energy. In comparison, FA 30% exhibits the slowest accumulation rate, suggesting that drag forces dominate and may lead to particle stratification or settling along the pipe base. This trend is consistent, as illustrated in Figure (b), FA 50% reaches the highest average particle velocity, exceeding 4 m/s, followed by FA 40% (approximately 3.2 m/s) and FA 30% (around 2.3 m/s). This velocity gradient highlights the effect of solid concentration on particle acceleration—greater Cw leads to enhanced hydrodynamic propulsion and increased mass transfer. Elevated particle velocity also increases the probability and severity of collisions with the wall.

The *Turbulent Kinetic Energy (TKE)* [Figure (c)] shows a clear escalation in kinetic energy with increasing concentration. FA 50% attains the highest kinetic energy (0.0863673), almost twice that of FA 40% (0.0561258) and quadruple that of FA 30% (0.0185431). This parameter reflects both the internal motion of particles and their interactive dynamics with the carrier fluid. Elevated kinetic energy is indicative of vigorous momentum exchange, thereby increasing the risk of material erosion at the pipe wall. Figure (d) reveals that although FA 50% exhibits superior kinetic parameters, the most severe wall wear occurs under FA 40% conditions, particularly toward the end of the simulation.

Figure (e) captures vertical upward forces acting on the pipe wall. Both the FA 40% and the FA 50% approaches yield magnitudes of approximately 2.5e-8 N, suggesting considerable particle suspension and collision above the flow centerline. Conversely, FA 30% shows minimal force, consistent with a lower-energy regime in which particles remain closer to the bottom boundary layer. In contrast, Figure (f) depicts the downward impact exerted by particles. FA 40% again shows the highest negative Z-axis force (~-1.2e-8 N), indicating that collisions with the lower pipe wall are more forceful under this condition. This contributes directly to abrasive wear at the pipe base and reflects the combined effect of velocity, turbulence, and particle mass.

The spatial distribution of erosion illustrates contrasting effects across different concentrations. In FA 30% (g), erosion is minimal and highly localized near the inlet zone. FA 40% (h) displays a wide and deep erosion track extending halfway down the pipe, indicating more aggressive and focused particle wall interactions. FA 50% (i), while showing a more dispersed erosion pattern, registers slightly lower maximum intensity than FA 40%. This supports the interpretation that FA 40% represents the most erosive condition, balancing high particle energy with

e-ISSN 2623-0313
p-ISSN 3032-1972

sufficiently chaotic flow to produce intensified wall stress.

Although a higher solid volume fraction enhances particle velocity, transit, and kinetic activity, the highest erosion rate does not necessarily correspond to the maximum concentration. FA 40% emerges as a critical operational point at which erosion potential is maximized, driven by the convergence of moderate energy, high particle-interaction frequency, and directional impact forces. In the context of circular pipe design, this finding underscores the importance of identifying concentration thresholds where hydrodynamic forces optimize particle momentum for erosion without exceeding material tolerance limits.

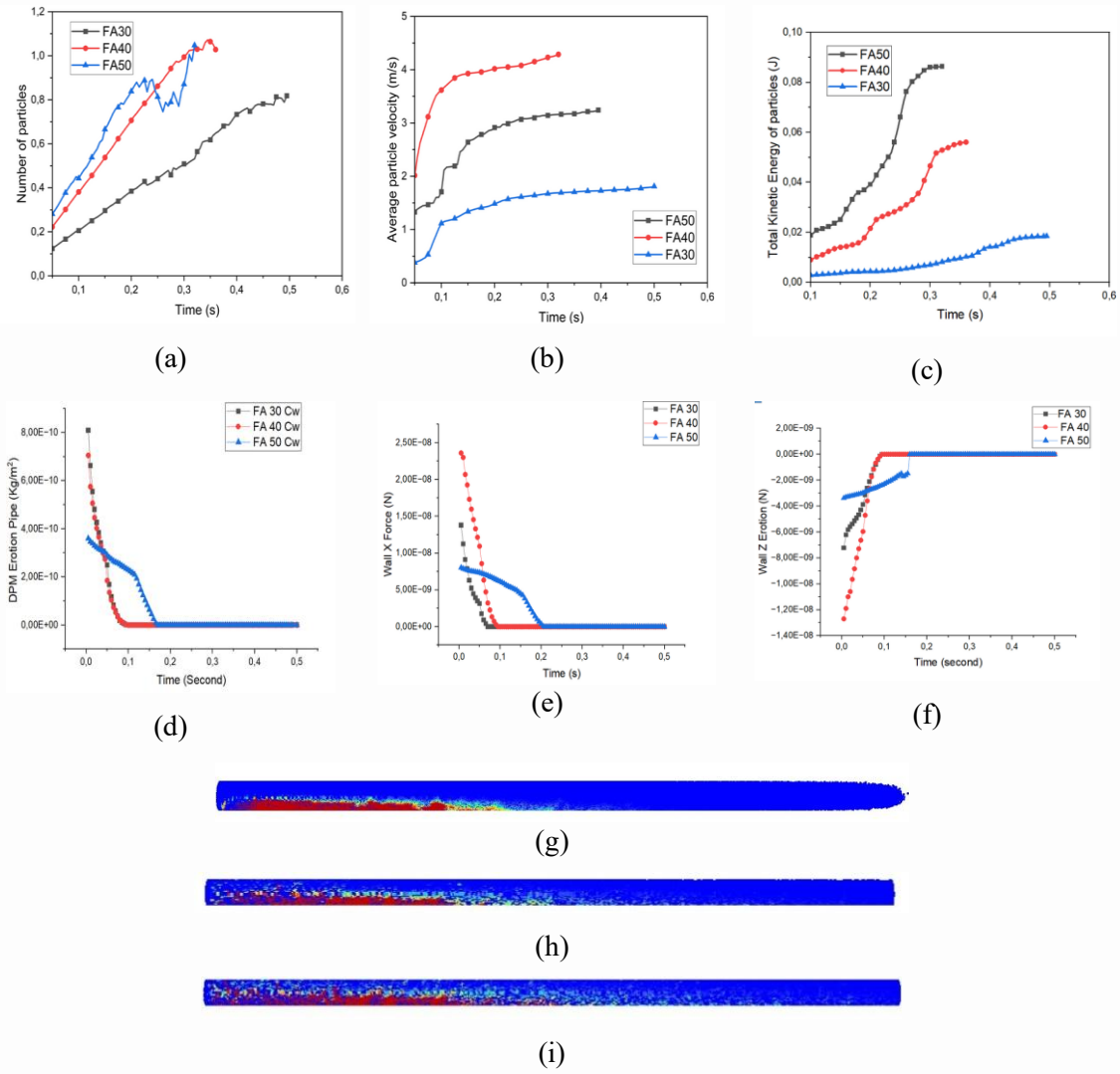

Figure 9. Schemes follow another format. If there are multiple panels, they should be listed as: (a) Particle X Position vs Time; (b) Particle Velocity vs Time; (c) Turbulent Kinetic Energy vs Time; (d) Graph of Fly Ash DPM Erosion in Circular Pipe; (e) Wall X Forces vs Time; (f) Wall Z Forces vs Time.; (g) Erosion of Fly Ash 30% CW in Circular Pipe; (h) Erosion of Fly Ash 40% CW in Circular Pipe; (i) Erosion of Fly Ash 50% CW in Circular Pipe

CONCLUSION

This study confirms that circular pipes can transport fly ash slurry effectively at high concentrations under turbulent conditions (Re = 50,000). The CFD–DEM model showed strong agreement with experiments, with deviations of 6.21%, 4.16%, and 5.03% at 30%, 40%, and 50% CW, respectively. The Grid Convergence Index of 0.017% further verified the accuracy of the simulations. Energy demand increased with rising solid concentration. At 30% CW, the pressure drop was the lowest (≈652 Pa), but turbulence was too weak to maintain suspension, raising the risk of sedimentation. At 40% CW, the pressure drop increased to 2,660 Pa, creating enough turbulence to keep particles suspended while avoiding excessive energy losses. At 50% CW, the pressure drop reached 3,251 Pa and TKE peaked at 0.086, about four times higher than at 30% CW indicating dense turbulent flow with strong particle–wall interactions. Erosion results followed this trend. At 30% CW, erosion was minimal and localized near the inlet. At 50% CW, erosion was

e-ISSN 2623-0313
p-ISSN 3032-1972

more dispersed but less intense. The most severe erosion occurred at 40% CW, where concentrated particle collisions and the highest downward impact forces (-1.2×10^{-8} N) created a deep erosion track along the lower pipe wall. Overall, 40% CW emerged as the most efficient but also the most critical operating condition. It balanced energy use and particle suspension while generating the highest erosion risk. These findings highlight the importance of CFD–DEM for pipeline design and the need to combine efficiency improvements with erosion-control strategies.

CREDIT AUTHORSHIP CONTRIBUTION

Yanuar: Conceptualization; methodology; validation; writing—original draft; writing—review and editing. Raja Fatah Satrio Abimanyu: Supervision; validation; review and editing. Gunawan: Conceptualization; methodology; validation; writing—original draft; writing—review and editing. Sri Poernomo Sari: Supervision; validation; review and editing. Chakra Merdeka: validation; review and editing.

ACKNOWLEDMENT

This work was supported by the Ministry of Education, Culture, Research, and Technology (Kemendikbudristek) of Indonesia through the PMDSU Research Grant No. NKB-969/UN2.RST/HKP.05.00/2024.

REFERENCE

[1] J. Gasparotto and K. Martinello, "Coal as an energy source and its impacts on human health," *Energy Geoscience,* vol. 2, 07/01 2020, doi: 10.1016/j.engeos.2020.07.003.

[2] A. Rokhmawati, A. Sugiyono, Y. Efni, and R. Wasnury, "Quantifying social costs of coal-fired power plant generation," *Geography and Sustainability,* vol. 4, no. 1, pp. 39-48, 2023/03/01/ 2023, doi: https://doi.org/10.1016/j.geosus.2022.12.004.

[3] M. Helios, S. Pipatmanomai, and S. Nasir, *Energy and Exergy Analysis of Coal-Fired Power Plants: The Selected Case Studies in Thailand and Indonesia*. 2012.

[4] M. Soleh, Y. Hidayat, and Z. Abidin, *Development of Coal Fired Power Plant Aging Fly Ash and Bottom Ash Utilization*. 2019, pp. 1-5.

[5] I. M. Widyarsana, S. Tambunan, and A. Mulyadi, *Identification of Fly Ash and Bottom Ash (FABA) Hazardous Waste Generation From the Industrial Sector and Its Reduction Management in Indonesia*. 2021.

[6] D. Das *et al.*, "Stabilization and Rheological Behavior of Fly Ash–Water Slurry Using a Natural Dispersant in Pipeline Transportation," *ACS Omega,* vol. 4, no. 25, pp. 21604-21611, 2019/12/17 2019, doi: 10.1021/acsomega.9b03477.

[7] S. Chandel, S. N. Singh, and V. Seshadri, "Deposition characteristics of coal ash slurries at higher concentrations," *Advanced Powder Technology,* vol. 20, no. 4, pp. 383-389, 2009/07/01/ 2009, doi: https://doi.org/10.1016/j.apt.2009.06.004.

[8] Y. Yanuar, K. Waskito, S. Mau, W. Wulandari, and S. Sari, "Helical twisted effect of spiral pipe in generating swirl flow for coal slurries conveyance," *Jurnal Teknologi,* vol. 79, 11/20 2017, doi: 10.11113/jt.v79.11899.

[9] M. Asof, S. Rachman, L. Luthfia, W. Andalia, and M. Naswir, "Analisis karakteristik dan potensi logam pada limbah padat fly ash dan bottom ash di PLTU industri pupuk," *Jurnal Teknik Kimia,* vol. 28, pp. 44-50, 03/01 2022, doi: 10.36706/jtk.v28i2.977.

[10] X. Ting, Z. Xinzhuo, S. A. Miedema, and C. Xiuhan, "Study of the characteristics of the flow regimes and dynamics of coarse particles in pipeline transportation," *Powder Technology,* vol. 347, pp. 148-158, 2019/04/01/ 2019, doi: https://doi.org/10.1016/j.powtec.2019.02.031.

[11] X. Zhang and G. Ahmadi, "Eulerian-Lagrangian Simulations of Liquid-Gas-Solid Flows in Three-Phase Slurry Reactors," *Chemical Engineering Science,* vol. 60, pp. 5089-5104, 09/01 2005, doi: 10.1016/j.ces.2005.04.033.

[12] J. Yang, B. Yang, and M. Yu, "Pressure Study on Pipe Transportation Associated with Cemented Coal Gangue Fly-Ash Backfill Slurry," *Applied Sciences,* vol. 9, p. 512, 02/02 2019, doi: 10.3390/app9030512.

[13] R. F. S. Abimanyu, Y. Yanuar, K. T. Waskito, W. R. Sari, and S. Ogata, "Impact of Reynolds Number on Flow Behavior in Spiral Pipe Profiles: A Review," *Journal of Advanced Research in Fluid Mechanics and Thermal Sciences,* vol. 129, no. 2, pp. 216-243, 04/10 2025, doi: 10.37934/arfmts.129.2.216243.

[14] F. Rayhan and Y. Yanuar, "Rheological behavior and drag reduction characteristics of ice slurry flow in spiral pipes," *Thermal Science and Engineering Progress,* vol. 20, p. 100734, 12/01 2020, doi: 10.1016/j.tsep.2020.100734.

e-ISSN 2623-0313
p-ISSN 3032-1972

[15] S. Huang, X. Su, and G. Qiu, "Transient numerical simulation for solid-liquid flow in a centrifugal pump by DEM-CFD coupling," *Engineering Applications of Computational Fluid Mechanics,* vol. 9, pp. 411-418, 01/01 2015, doi: 10.1080/19942060.2015.1048619.

[16] W. Pu *et al.*, "Study on the particle dynamic characteristics in a centrifugal pump based on an improved computational fluid dynamics-discrete element model," *Physics of Fluids,* vol. 36, 12/06 2024, doi: 10.1063/5.0242078.

[17] R. Zhao, Y. Zhou, Z. Desheng, and X. Gao, "Numerical investigation of the hydraulic transport of coarse particles in a vertical pipe based on a fully-coupled numerical model," *International Journal of Multiphase Flow,* vol. 155, p. 104094, 04/01 2022, doi: 10.1016/j.ijmultiphaseflow.2022.104094.

[18] H. Zhu, Z. Zhou, R. Yang, and A. Yu, "Discrete particle simulation of particulate systems: A review of major applications and findings," *Chemical Engineering Science - CHEM ENG SCI,* vol. 63, pp. 5728-5770, 12/01 2008, doi: 10.1016/j.ces.2008.08.006.

[19] B. Mishra, S. Rai, K. Gavhane, and M. Deshpande, "Turbulence Modeling in Navier-Stokes Equations: Challenges and Approaches," *International Research Journal of Modernization in Engineering Technology and Science,* vol. 06, p. 964, 04/23 2024, doi: 10.56726/IRJMETS53610.

[20] M. ten Eikelder, "A unified framework for N-phase Navier–Stokes Cahn–Hilliard Allen–Cahn mixture models with non-matching densities," *Journal of Fluid Mechanics,* vol. 1013, 06/19 2025, doi: 10.1017/jfm.2025.10186.

[21] C. Sun *et al.*, "Study of hydraulic transport characteristics and erosion wear of twisted four-lobed pipe based on CFD-DEM," *Particuology,* vol. 95, pp. 356-369, 2024/12/01/ 2024, doi: https://doi.org/10.1016/j.partic.2024.10.011.